Composites: Part A 54 (2013) 173–181

Contents lists available at ScienceDirect

Composites: Part A

journal homepage: www.elsevier.com/locate/compositesa

Effects of plasma modified carbon nanotube interlaminar coating on crack propagation in glass epoxy composites

John Williams [a,*], Neil Graddage [b], Sameer Rahatekar [a,*]

[a] ACCIS, Dept. Aerospace Engineering, University of Bristol, Bristol BS8 1TR, United Kingdom
[b] Welsh Centre for Printing and Coating, Swansea University, Swansea SA2 8PP, United Kingdom

ARTICLE INFO

Article history:
Received 10 July 2013
Accepted 29 July 2013
Available online 6 August 2013

Keywords:
A. Polymer–matrix composites (PMCs)
A. Particle-reinforcement
B. Fracture toughness
D. Mechanical testing

ABSTRACT

Fibre reinforced pre-preg systems have very good in plane properties, however they are weak in their through thickness (*z*) direction. This research aims to address this issue by adding plasma treated carbon nanotubes (CNTs) between the prepreg plies using a simple drawdown coating procedure. The significant test result shows by coating carbon nanotubes with a relatively low areal density (1.2 g/m^2) the propagation mode I toughness can be improved by up to 46%. Crack deviation leading to increased glass fibre bridging was observed for lower CNT coating concentrations explaining the improved performance. However at the highest areal coating density (2.0 g/m^2) fibre bridging disappeared and a stick–slip crack response was observed resulting in lower delamination resistance. This research demonstrates a simple method to incorporate a nanointerlayer that can manipulate crack propagation, leading to increased delamination resistance.

1. Introduction

Fibre reinforced composites have excellent in plane strength and stiffness to weight ratio properties and are being used in increasing quantities in aerospace and automotive industries. However fibre reinforced composites are weak in their through thickness direction. This weakness can result in parts failing by delamination in service, either from external loads or impact events. The presence of a delamination can seriously reduce the strength and stiffness of a laminate especially under compressive buckling loads, potentially leading to catastrophic failure [1]. This research aims to address this issue by using a carbon nanotube interlayer between pre-preg plies to increase the delamination resistance.

Strategies do exist for directly addressing the delamination problem, the most common ones being Z-pinning, 3D Weaving, toughening particles, short fibres and interleaving tough layers between the plies. These methods work on the macro scale and each method has its own advantages and disadvantages compared to the nanoscale reinforcement presented in this study. For example Z-pinning [2–6] is known to give large improvements in delamination resistance, but at the cost of reduced in plane properties as the pins acting like nails can damage fibres and add to fibre waviness. 3D woven composites [7,8] as well as interleaving tough layers [9–15] can improve the delamination resistance but again at the cost of reduced in plane properties.

Carbon nanotubes have been shown individually to be extremely strong, stiff and tough [16–18] and should make excellent candidates as reinforcements for a polymer. However commercial grades of carbon nanotubes come in a powder form of highly entangled nanotubes, added to this their large surface areas [19] and low surface energy makes them difficult to disperse evenly within a solvent or polymer [20]. Due to this reason, some pretreatment to the CNTs is needed such as acid [21–24], or dispersants [25–27] to improve compatibility with the host matrix.

Plasma treatment of carbon nanotubes [28–31] offers an alternative to wet chemistry methods and has the advantages of being dry, single step processing, controllable, quick and, highly flexible in terms of the variety of gases available which can give different functionalities.

Carbon nanotubes as a reinforcement has previously been shown as an effective method for reinforcing an epoxy polymer [20,32] and further developments have been made incorporating CNTs into fibre reinforced composites with varying success [33–37].

We have developed a novel method of plasma treatment [31] of commercial grade carbon nanotubes which is shown to improve dispersion of CNTs in epoxy and are now applying this work to traditional glass reinforced epoxy composite materials. This study uses a drawdown process on aerospace grade prepreg as an alternative manufacturing technique which is simpler than previously

* Corresponding authors. Tel.: +44 1173315330.
E-mail addresses: John.David.Williams@Bristol.ac.uk (J. Williams), Sameer.Rahatekar@Bristol.ac.uk (S. Rahatekar).

1359-835X
http://dx.doi.org/10.1016/j.compositesa.2013.07.018

Table 1
Ethanol constants at 25 °C [48].

Solvent	Viscosity η mPa s	Dielectric constant ϵ
Ethanol	1.074	24.85

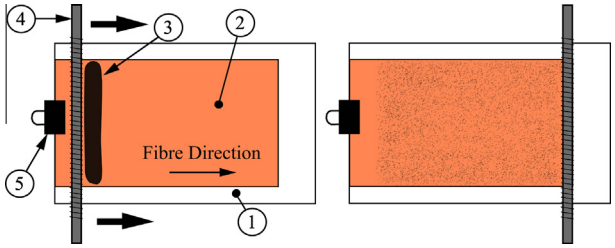

Fig. 1. Drawdown coating: (1) Glass, (2) Pre-preg, (3) CNT ethanol solution, (4) Drawbar, (5) Clip. (For interpretation of the references to colour in this figure legend, the reader is referred to the web version of this article.)

presented methods for incorporating a nanofiller into a composite system. The process is quick, single step, potentially scalable and negates CNT filtering problems and increased viscosity associated with resin transfer moulding methods [38]. We also show that the fracture behaviour can be completely modified by the filler quantity and consequently result in higher or lower fracture toughness.

2. Experimental

2.1. Materials

2.1.1. Carbon nanotubes

Bayer Material Science C150P carbon nanotubes [39] have been used for this study. The C150P nanotubes are a commercial grade of high purity $\geqslant$95%, multiwalled carbon nanotubes and come in an agglomerated powder form. To improve their stability in common solvents, they have been oxygen plasma treated by Haydale [40]. The carbon nanotubes are treated in a specially modified plasma reactor, suitable for handling large quantities of nanomaterial, see patents [41,42]. Our previous research [31] indicates this oxygen treatment adds carboxylic acid groups to the carbon nanotubes at 2.97 wt.%, increases the free surface energy and reduces the bulk density.

2.1.2. Pre-preg system

Hexcel E-Glass 913 [43] unidirectional pre-preg system has been used though out this study to characterise the affects of a carbon nanotube coating on mode I fracture toughness.

2.2. Zeta potential

To characterise the stability of the solutions, zeta potential measurements have been made. The solution preparation was as follows, 0.02 g of the CNT powders were added to 25 ml of ethanol in a bottle. The bottles were shaken by hand in a consistent manner. The solutions were allowed to settle for 10 min before taking a sample of the supernatant with a syringe. The supernatant was then injected into the folded capillary cell ready for measurement on a Malvern Zetasizer Nano Z system. The system directly measures electrophoretic mobility (μ_E), the velocity of the suspended particles in solution within an electric field, achieved by laser Doppler velocimetry. Using the solvent properties (Table 1), the electrophoretic mobility and the Henry Eq. (1) [44], the zeta potential can be calculated. These calculations were done by the Zetasizer software [45]. All measurements were conducted at 25 °C, where U_E is the electrophoretic mobility, ϵ the solution dielectric constant, ζ zeta potential, η viscosity and $f(ka)$ Henry's function which increases from 1.0 at $ka = 0$ to 1.50 at $ka = \infty$ for this study taken as 1.5 (Smoluchowski approximation) as used by similar studies [46,47]. This approach makes the assumption that the particles are spherical which is not the case for carbon nanotubes consequently this method can over estimate the true zeta potential by 20% [47].

$$U_E = \frac{2\varepsilon\zeta f(ka)}{3\eta} \tag{1}$$

Table 2
Coating density.

Solution concentration	Measured coating density
0.5 g/30 ml	1.2 g/m^2
1.0 g/30 ml	1.6 g/m^2
1.5 g/30 ml	2.0 g/m^2

Table 3
Zeta potential results.

Material	ζpotential
C150P-untreated	2.9
C150P-oxygen treated	−31.5

2.3. Specimen manufacture

The coating of the CNTs onto glass fibre pre-preg was as follows. Oxygen plasma treated carbon nanotubes were dispersed in 30 ml of ethanol at 0.5 g, 1.0 g and 1.5 g concentrations. These solutions were then vortex mixed using a IKA MS 3 Basic. This solution was then dispensed onto the top edge of the pre-preg (Hexcel E-Glass 913) using a pipette. Using a drawdown bar (wire gauge 0.5 mm) without rolling the bar, the solution was drawn down the prepreg giving a coating of cabon nanotubes, an illustration of the drawdown coating procedure is shown in Fig. 1. The ethanol was then allowed to evaporate off before another ply is placed on top and the process is repeated again. The

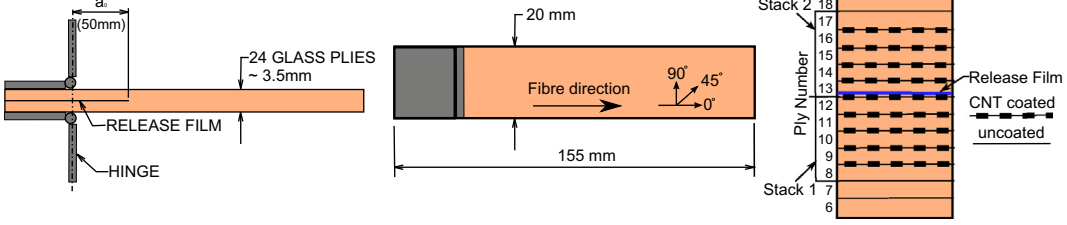

Fig. 2. DCB test geometry and schematic indicating which plies have been CNT coated. (For interpretation of the references to colour in this figure legend, the reader is referred to the web version of this article.)

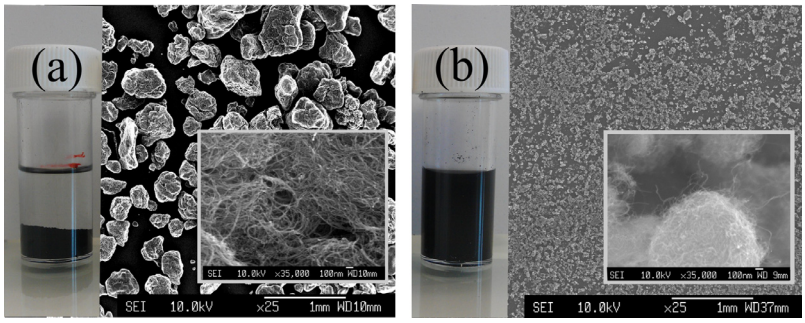

(a) Untreated CNTs. (b) Oxygen Plasma treated CNTs.

Fig. 3. Solution stability and morphology comparison between the untreated and treated CNTs. (For interpretation of the references to colour in this figure legend, the reader is referred to the web version of this article.)

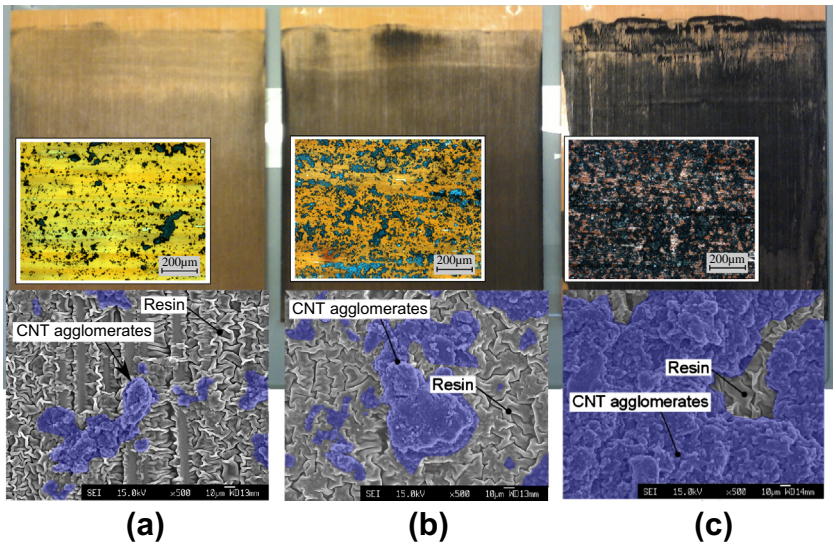

Fig. 4. Pre-preg coatings (a) 1.2 g/m^2 (b) 1.6 g/m^2 (c) 2.0 g/m^2. Micrograph inserts show respective CNT deposits on the pre-preg. The SEM images shows added detail of the resin texture and CNT agglomerates highlighted blue for clarity. (For interpretation of the references to colour in this figure legend, the reader is referred to the web version of this article.)

stacking process was repeated in parallel until two stacks of five plies are completed with only one of the stacks having a top coating (Fig. 2 Stack 1) with a sheet of release film on top of the CNT coating forming the artificial crack. Stack 2 is then laid on top, locking the release film in the middle, creating a stack of ten plies, nine of which have been coated. It was decided to coat the nine central plies as it was unknown at the time to what extent the CNTs would migrate during the curing process. Another seven uncoated plies are then added either side of the stack to produce a 24 ply laminate all at 0°. The laminate is then bagged and cured in an autoclave in accordance with the manufacturers curing schedule (125 °C for 1 h at 7 Bar) with an added dwell to reduce any exotherm. Once the laminate is cured, 10 mm is cut off around all the edges. Double cantilever beam (DCB) specimens are then cut in accordance with the ASTM D5528-01 [49] standard (width $b = 20$ mm, crack length $a_0 = 50$ mm $L = 155$ mm) see Fig. 2 for details and a schematic identifying which central plies have been CNT coated. Piano hinges were also attached as indicated in Fig. 2 to facilitate loading using Redux 810 adhesive. Table 2 shows the three different solution concentrations used and the resulting coating density.

2.4. Testing procedure

Double cantilever beam testing to determine mode I fracture toughness was carried out in accordance to ASTM D5528-01 [49] using an Instron 3343 testing machine and a 1 kN load cell. The crosshead displacement speed was set at 2 mm/min. The crack growth was monitored using a digital video camera. The energy release rate (G_{1c}) was calculated using the modified beam theory method Eq. (2). The initiation value of G_{1c} has been made using the 5% offset maximum load method, as it is not relent upon visual interpretation to determine when the crack starts to grow. The propagation value has been determined by averaging the G_{1c} values between crack lengths of 80 mm up to 105 mm. The flexural modulus has also been calculated in accordance with ASTM D5528-01 using Eq. (3). Where P: the load, δ: the load point displacement, b: the specimen width, a: the delamination length, h: the specimen thickness and Δ: correction factor to account for rotation of the DCB arms. Δ: was determined experimentally in accordance with ASTM D5528-01 by generating a least squares plot of the cube root of compliance ($C^{1/3}$) as a function of delamination length.

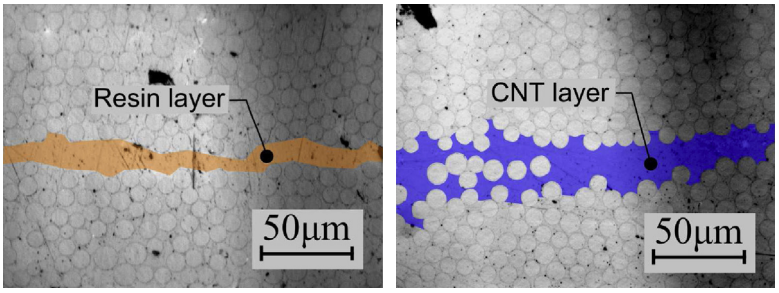

(a) Glass control. (b) 1.2g/m^2 coated.

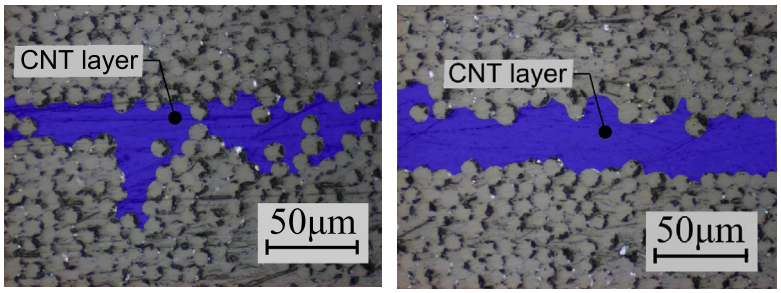

(c) 1.6g/m^2 coated. (d) 2.0g/m^2 coated.

Fig. 5. Micrographs of specimen cross sections, view looking at the ends of the fibres. Ply interface regions highlighted. Colour added for clarity. Orange: 913 resin interlayer, Blue: Carbon Nanotube/ 913 resin interlayer. (For interpretation of the references to colour in this figure legend, the reader is referred to the web version of this article.)

$$G_{1c} = \frac{3P\delta}{2b(a+|\Delta|)} \tag{2}$$

$$E_{if} = \frac{64(a+|\Delta|)^3 P}{\delta b h^3} \tag{3}$$

3. Results

3.1. Zeta potential

The zeta potential results from the study are shown in Table 3. A visual interpretation of the zeta potential results is shown in the Fig. 3 inserts of the CNT ethanol solutions. The quick settling untreated CNTs have a low magnitude of zeta potential whilst the plasma treated CNTs show a higher zeta potential magnitude indicating much better stability. The negative zeta potential sign for the C150P oxygen plasma treated sample indicates that these CNTs are negatively charged in the ethanol solution. These results are similar to previous finding [50–53] for acid treated CNTs showing higher magnitude zeta potentials compared to untreated CNTs, but obtained using a much simpler plasma process. The SEM images of the carbon nanotubes Fig. 3 shows a large reduction in agglomerate size post plasma treatment, although the treatment has not completely unbound the agglomerates into individual CNTs, the

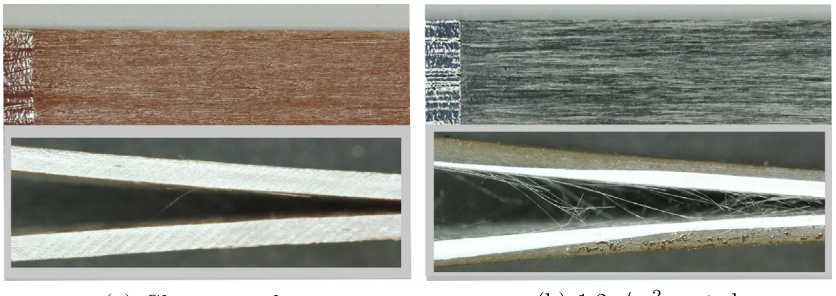

(a) Glass control. (b) 1.2g/m^2 coated.

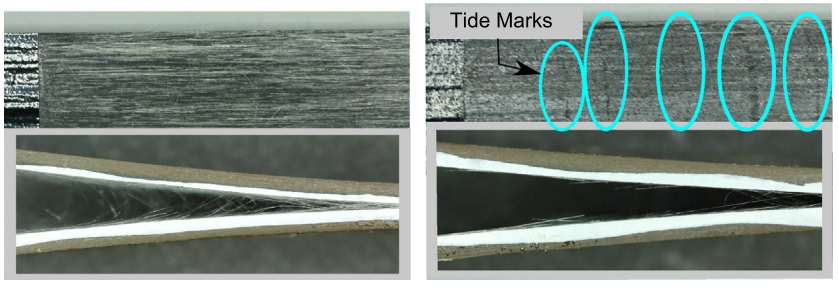

(c) 1.6g/m^2 coated. (d) 2.0g/m^2 coated.

Fig. 6. Images of typical DCB specimens showing fracture surfaces and open DCB specimens, highlighting the observed differences in fibre bridging behaviour and fracture surface textures. (For interpretation of the references to colour in this figure legend, the reader is referred to the web version of this article.)

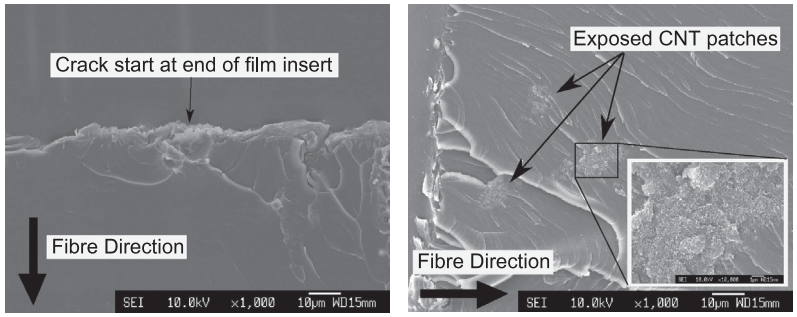

(a) Glass control, image showing a standard fracture surface.

(b) 1.2g/m^2 coated surface showing sparse patches of carbon nanotubes in the matrix.

(c) 1.6g/m^2 coated surface showing an increased quantity of carbon nanotube clusters.

(d) 2.0g/m^2 coated surface showing a high density of visable carbon nanotubes.

Fig. 7. SEM images of the fracture surfaces around the crack initiation site, highlighting the increase in exposed CNTs between the specimens after a crack has propagated through.

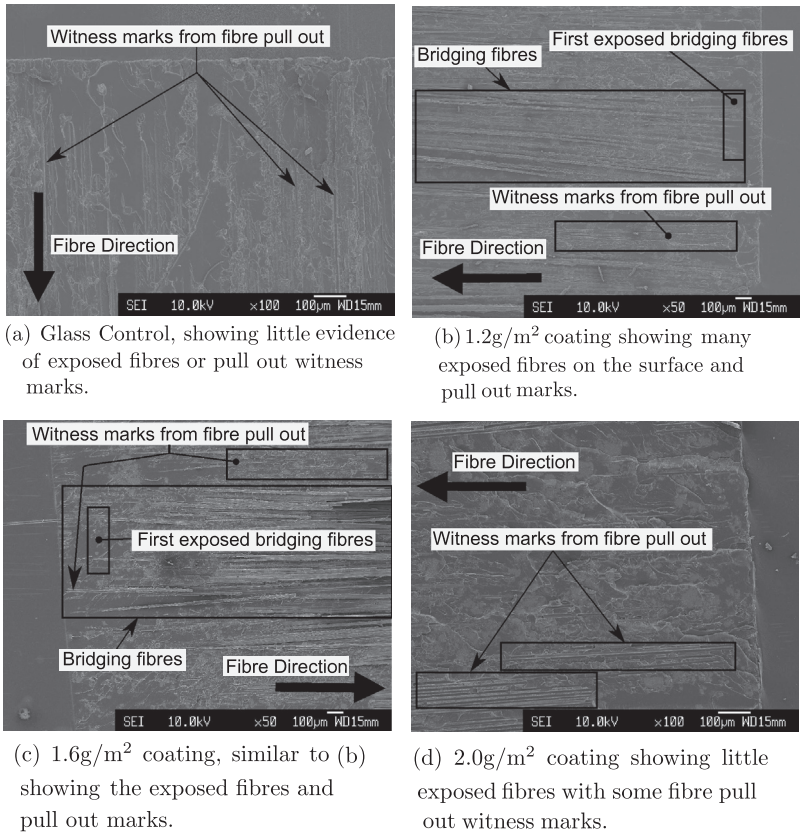

(a) Glass Control, showing little evidence of exposed fibres or pull out witness marks.

(b) 1.2g/m^2 coating showing many exposed fibres on the surface and pull out marks.

(c) 1.6g/m^2 coating, similar to (b) showing the exposed fibres and pull out marks.

(d) 2.0g/m^2 coating showing little exposed fibres with some fibre pull out witness marks.

Fig. 8. SEM images of the fracture surfaces beyond crack tip, fibre direction, exposed glass fibres and witness marks left behind from pulled out fibres highlighted.

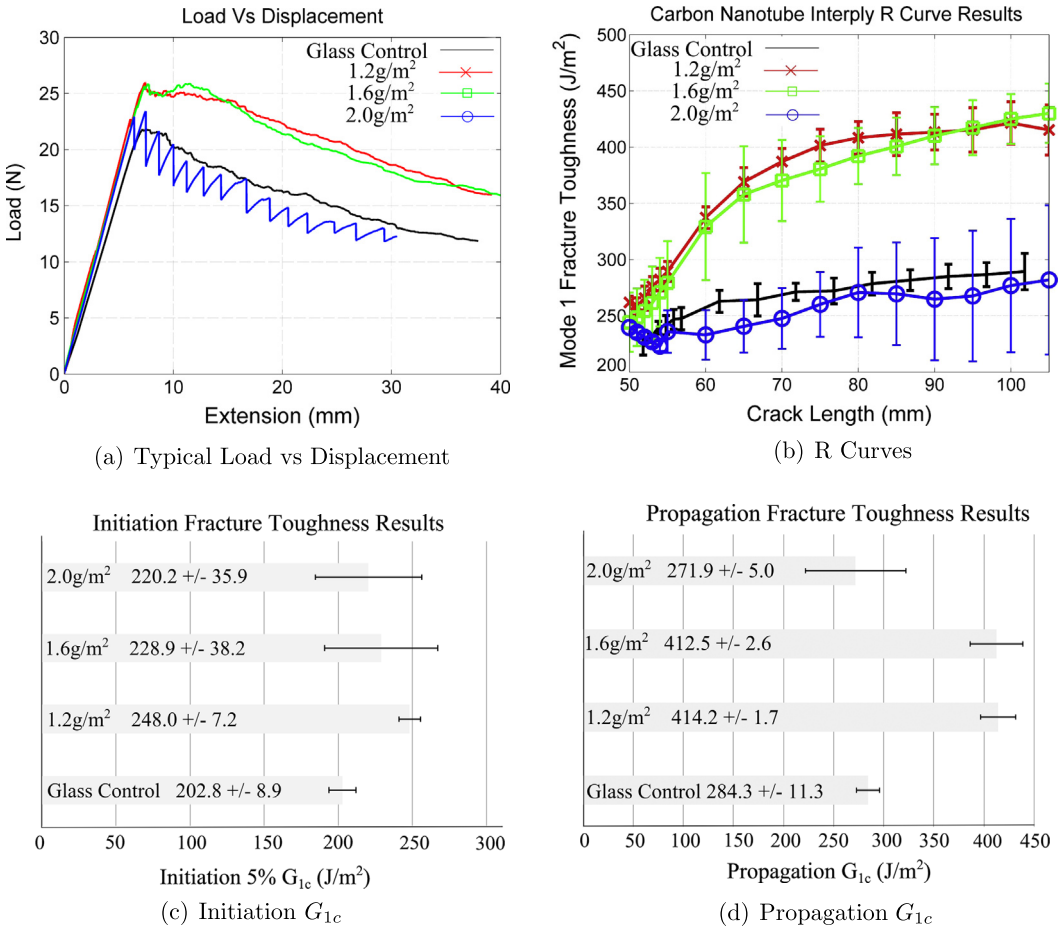

(a) Typical Load vs Displacement

(b) R Curves

(c) Initiation G_{1c}

(d) Propagation G_{1c}

Fig. 9. Mode I, mechanical testing results (error bars show ± one standard deviation). (For interpretation of the references to colour in this figure legend, the reader is referred to the web version of this article.)

combination of reduced agglomerate size and added oxygen functionality [31] have improved stability.

3.2. Pre-preg coating quality

Fig. 4 shows the nanotube coatings on the pre-pregs, in each case it is possible to see the solution dwell at the top of the samples. It should be noted this does not affect the DCB testing as the crack is initiated far below the dwell area. The micrograph Fig. 4 inserts show a contrast from sparse to dense deposition of the CNTs to the pre-preg material consistent with increased coating solution concentration. The SEM images of the CNT coated pre-preg surfaces were silver sputtered for imaging, they show an uneven resin texture with the increasing quantity of CNT agglomerates attached to the surface, highlighted in blue for clarity. The 1.2 g/m^2 and 1.6 g/m^{2}solutions drew down well compared to the 2.0 g/m^2 solution, which produced a coarse much more continuous coating.

3.3. The cured carbon nanotube layer

From visual inspection the CNT layers tend to stay put although a shallow migration above and below a few layers of fibres is seen. Fig. 5 shows example cross sections of the specimens, Fig. 5a of the glass control has shown areas of a definable boundary between the plies but not necessarily continuous, whilst compared to Fig. 5d of the 2.0 g/m^2 coated sample shows a clear continuous boundary. The 1.2 g/m^2 coating was similar to the 1.6 g/m^2 coating Fig. 5b and c displaying an interface region, but not as well defined as glass fibres can be seen within the inter-ply region. The width of CNT interply region was found to be 12.57 μm ± 5.35, 16.08 μm ± 6.35 and 23.50 μm ± 7.89, for the 1.2 g/m^2,1.6 g/m^2 and, 2.0 g/m^2 coatings respectfully. The large standard deviations shows how much this interply region varies along its length and how difficult it can be to define.

3.4. Fracture surface

Fig. 6 shows the crack planes of the fractured DCB specimens and a view showing the typical bridging response. The 1.2 g/m^2 and 1.6 g/m^2 coated pre-pregs have preformed similarly, of importance to note is the wool like texture on their crack planes and that they display much more fibre bridging compared to the glass control Fig. 6a and the 2.0 g/m^2 specimen Fig. 6d coated specimen. The 2.0 g/m^2 Fig. 6d test specimens displayed tide marks, highlighted by ovals where the crack has propagated rapidly by sticking and

Table 4
Flexural modulus parenthesis show one standard deviation.

Name	Flexural modulus (GPa)
1.5 g Coating	45.6 ± (6.4)
1.0 g Coating	45.7 ± (2.2)
0.5 g Coating	45.4 ± (1.2)
Glass control	45.1 ± (2.7)

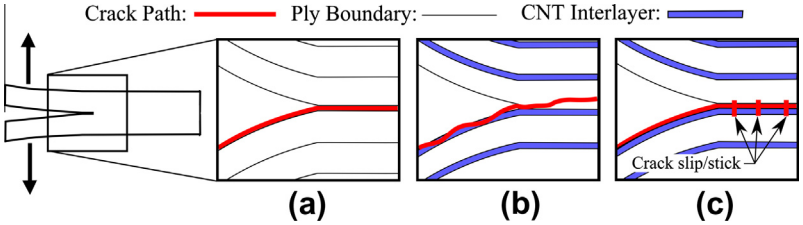

Fig. 10. DCB crack propagation modes: (a) glass control crack propagating between the plies. (b) 1.2 g/m^2 and 1.6 g/m^2 coated, showing deflected crack propagating within a ply (c) 2.0 g/m^2 coating, crack slips and sticks along CNT ply interface at various intervals creating tide marks. (For interpretation of the references to colour in this figure legend, the reader is referred to the web version of this article.)

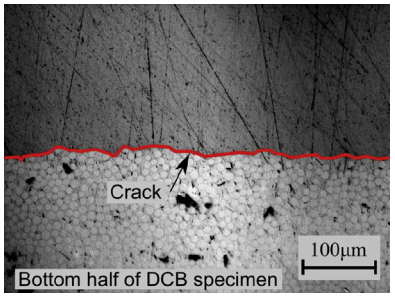

(a) Glass Control example showing a clean fracture.

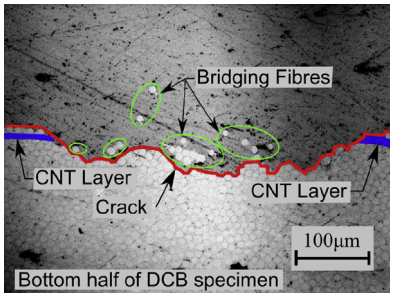

(b) 1.2g/m^2, coated example 1.6g/m^2 similar, showing complex crack path with bridging fibres.

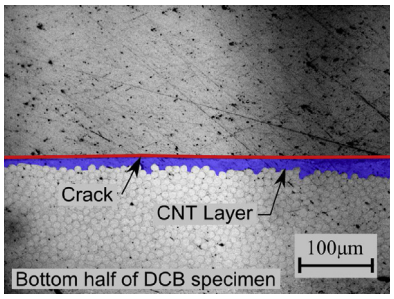

(c) 2.0g/m^2 coated sample, showing crack propagating along the top of the CNT inter layer.

Fig. 11. Micrograph images after fracture, viewing down the fibre direction. Showing the differing responses between the samples. Colour added for clarity. Red: Fracture plane, Green: Bridging Fibres, Blue: Nanotube interlayer. (For interpretation of the references to colour in this figure legend, the reader is referred to the web version of this article.)

slipping. The tide marks on closer inspection are areas of exposed fibres, indicating a short directional change in the crack path.

3.5. SEM fracture surface images

The SEM images in Fig. 7 shows the fracture surface near the film insert. The arrows indicate the fibre direction as well as the crack propagation direction. The SEM of the glass control Fig. 7a specimen has a much smoother appearance compared to the CNT filled specimens. In Fig. 7b–d the dense carbon nanotube areas that have been revealed during the fracture process are highlighted, whilst the insert images show a close up of a CNT rich region. The observable coverage of the CNTs on the surface increases with the coating concentration as expected.

SEM images in Fig. 8 shows the fracture surfaces beyond the crack initiation area. It is possible to see much more exposed fibres in the 1.2 g/m^2 and 1.6 g/m^2 CNT coated samples Fig. 8b and c compared to the glass control and 2.0 g/m^2 coated specimens Fig. 8a and d, corroborating what is observable in Fig. 6 of the differing fracture plane textures. These SEM images also show that bridging does not start instantly from the crack tip and that the first exposed fibres appear approximately 100 μm from the initiation line.

3.6. Mechanical testing results

The complied test data is shown in Fig. 9. Typical load vs. displacement plots of each test piece is shown in Fig. 9a. The 1.2 g/m^2 and 1.6 g/m^2 sample perform fairly similarly and better than the glass control both in terms of initiation and load carrying capability. The 2.0 g/m^2 specimens however performed worse than the control in terms of propagation, but had a higher initiation load. The saw tooth behaviour of the 2.0 g/m^2 specimens is due to the slip and stick crack jumping during the testing. The delamination resistance curves '*R*' curves shown in Fig. 9b mimic what is seen in the load displacement graphs. That is the G_{1c} values are significantly higher for the 1.2 g/m^2 and 1.6 g/m^2 samples during propagation, compared to the glass control and 2.0 g/m^2 samples. The large error bars shown for the 2.0 g/m^2 specimen is due to the sporadic nature

of the crack jumping at different points between the samples. Fig. 9c and d contains a summary of the initiation and propagation results calculated from the tests and highlights the significant G_{1c} increases obtained by 1.2 g/m^2 and 1.6 g/m^2 coatings.

The flexural modulus presented in Table 4 has been averaged over the complete DCB testing regime as the values do vary slightly as the test progresses. It is important to note that the flexural modulus is almost unchanged between the samples. Although expected being a fibre dominated property.

3.7. Discussion

The oxygen plasma treatment previously developed in our group [31] has been an instrumental part of this study as it has allowed the production of a stable CNT ethanol solution which was vital for a successful drawdown process as it would be impossible to use untreated CNTs in this process due to their quick settling nature.

The drawdown coating of the pre-preg has shown to be an economical and effective way for creating multiscaled composites and could be used for adding a functional layer to composites. The process also negates the filtering affects and viscosity problems associated with resin transfer methods of creating multiscale composites [38]. The solution dwell noted in Section 3.2 could be avoided in a continuous process environment.

The increase in mode I fracture toughness can not be explained by the CNTs bulking the interply resin region alone, as at the largest coating density the fracture toughness actually reduces. It is evident however that for the more sparsely CNT coated specimens, crack deviation causing increased fibre bridging of the glass fibres is the primary reinforcing mechanism observed. A schematic of the observed differences in crack propagation between the test cases is shown in Fig. 10 and is based on the evidence from the micrographs shown in Fig. 11. The important difference is that for the 1.2 g/m^2 and 1.6 g/m^2 coated laminates is the crack has been diverted away from the mid plane and has propagated erratically within the ply resulting in clusters of fibres being pulled away and bridging Fig. 11b, in contrast the control case has a relatively clean crack line. In previous studies it has been seen that thickened interlayers and carbon nanotubes within a polymer can cause cracks to deflect [10,54], although in this case it is possible the more sparsely spread CNT agglomerates are acting like discrete voids or defects encouraging fibre bridging by allowing alternative crack paths to form [55–57]. The 2.0 g/m^2 coated specimens Fig. 11c differs again as the fracture occurs mainly along the top of the CNT-ply interface indicating a cohesive failure between the CNT layer and the adjacent prepreg which ultimately led to reduced performance and indicates a limit to performance that can be achieved by this method. It should be noted to the reader that the observed responses can be attributed to the CNT interlayer and not the drawdown procedure its self, as an ethanol only coated specimen behaved similarly to the glass control presented here, in terms of the quantity of fibre bridging and the resulting delamination resistance.

4. Conclusions

This report studied the affect of adding different quantities of carbon nanotubes as an interlayer between prepreg plies. The following can be highlighted from the study.

1. Oxygen plasma treatment is a useful method to improve the stability of the carbon nanotubes in ethanol and allows an ink like solution of CNTs to be made.
2. The drawdown technique has been shown to be a very effective alternative method for coating nanomaterial onto a prepreg surface.
3. Through the methods outlined in this study it has been shown possible to increase the fracture toughness of glass fibre prepreg up to 22% and 46% for initiation and propagation respectfully. However a limit has been reached and beyond a 1.6 g/m^2 coating the improvements are lost. This increase at the lower areal coating densities can be attributed to increased glass fibre bridging, which has occurred due to the crack being encouraged to propagate within the ply and not along the ply interface.

Acknowledgements

The authors thank the Engineering and Physical Sciences Research Council (EPSRC) for supporting the Advanced Composites Centre for Innovation and Science (ACCIS) Doctoral Training Centre (DTC), Grant No. EP/G036772/1. The Bristol Centre for Nanoscience and Quantum Information (NSQI) for the use of their specialist facilities in regards to handling and processing of the carbon nanotubes. Also many thanks Ian Walters and Martin Williams of Haydale Ltd. for their support.

References

[1] Cantwell W, Morton J. The impact resistance of composite materials: a review. Composites 1991;22:347–62.
[2] Mouritz A. Review of z-pinned composite laminates. Compos Part A: Appl Sci Manuf 2007;38:2383–97.
[3] Lenzi F, Riccio A, Clarke A, Creemers R. Coupon tests on z-pinned and unpinned composite samples for damage resistant applications. Macromol Sympos 2007;247:230–7.
[4] Partridge IK, Cartie DD. Delamination resistant laminates by z-fiber pinning: Part I manufacture and fracture performance. Compos Part A: Appl Sci Manuf 2005;36:55–64.
[5] Robinson P, Das S. Mode I DCB testing of composite laminates reinforced with z-direction pins: a simple model for the investigation of data reduction strategies. Eng Fract Mech 2004;71:345–64.
[6] Zhang X, Hounslow L, Grassi M. Improvement of low-velocity impact and compression-after-impact performance by z-fibre pinning. Compos Sci Technol 2006;66:2785–94.
[7] Mouritz A, Baini C, Herszberg I. Mode I interlaminar fracture toughness properties of advanced textile fibreglass composites. Compos Part A: Appl Sci Manuf 1999;30:859–70.
[8] Dransfield K, Baillie C, Mai Y-W. Improving the delamination resistance of CFRP by stitching a review. Compos Sci Technol 1994;50:305–17.
[9] Masters JE. Improved impact and delamination resistance through interleaving. Key Eng Mater 1991;37:317–48.
[10] Singh S, Partridge I. Mixed-mode fracture in an interleaved carbon-fibre/epoxy composite. Compos Sci Technol 1995;55:319–27.
[11] Sela N, Ishai O, Banks-Sills L. The effect of adhesive thickness on interlaminar fracture toughness of interleaved cfrp specimens. Composites 1989;20:257–64.
[12] Gibson RF, Chen Y, Zhao H. Improvement of vibration damping capacity and fracture toughness in composite laminates by the use of polymeric interleaves. J Eng Mater Technol 2001;123:309–14.
[13] Ozdil F, Carlsson LA. Mode I interlaminar fracture of interleaved graphite/epoxy. J Compos Mater 1992;26:432–59.
[14] Yasaee M, Bond I, Trask R, Greenhalgh E. Mode I interfacial toughening through discontinuous interleaves for damage suppression and control. Compos Part A: Appl Sci Manuf 2012;43:198–207.
[15] Yasaee M, Bond I, Trask R, Greenhalgh E. Mode II interfacial toughening through discontinuous interleaves for damage suppression and control. Compos Part A: Appl Sci Manuf 2012;43:121–8.
[16] Treacy MMJ, Ebbesen TW, Gibson JM. Exceptionally high young's modulus observed for individual carbon nanotubes. Nature 1996;381:678–80.
[17] Wong EW, Sheehan PE, Lieber CM. Nanobeam mechanics: elasticity, strength, and toughness of nanorods and nanotubes. Science 1997;277:1971–5.
[18] Salvetat-Delmotte J-P, Rubioh A. Mechanical properties of carbon nanotubes: a fiber digest for beginners. Carbon 2002;40:1729–34.
[19] Peigney A, Laurent C, Flahaut E, Bacsa R, Rousset A. Specific surface area of carbon nanotubes and bundles of carbon nanotubes. Carbon 2001;39:507–14.
[20] Gojny FH, Wichmann MH, Fiedler B, Schulte K. Influence of different carbon nanotubes on the mechanical properties of epoxy matrix composites a comparative study. Compos Sci Technol 2005;65:2300–13.
[21] Zhu J, Kim J, Peng H, Margrave JL, Khabashesku VN, Barrera EV. Improving the dispersion and integration of single-walled carbon nanotubes in epoxy composites through functionalization. Nano Lett 2003;3:1107–13.
[22] Kim SD, Kim JW, Im JS, Kim YH, Lee YS. A comparative study on properties of multi-walled carbon nanotubes (MWCNTs) modified with acids and oxyfluorination. J Fluor Chem 2007;128:60–4.

[23] Ma P-C, Siddiqui NA, Marom G, Kim J-K. Dispersion and functionalization of carbon nanotubes for polymer-based nanocomposites: a review. Compos Part A: Appl Sci Manuf 2010;41:1345–67.
[24] Kim YJ, Shin TS, Choi HD, Kwon JH, Chung Y-C, Yoon HG. Electrical conductivity of chemically modified multiwalled carbon nanotube/epoxy composites. Carbon 2005;43:23–30.
[25] Tkalya EE, Ghislandi M, de With G, Koning CE. The use of surfactants for dispersing carbon nanotubes and graphene to make conductive nanocomposites. Curr Opin Colloid Interface Sci 2012.
[26] Kim KH, Jo WH. Improvement of tensile properties of poly(methyl methacrylate) by dispersing multi-walled carbon nanotubes functionalized with poly(3-hexylthiophene)-graft-poly(methyl methacrylate). Compos Sci Technol 2008;68:2120–4.
[27] Loos M, Yang J, Feke D, Manas-Zloczower I. Effect of block-copolymsser dispersants on properties of carbon nanotube/epoxy systems. Compos Sci Technol 2012;72:482–8.
[28] Felten A, Bittencourt C, Pireaux JJ, Lier GV, Charlier JC, et al. Radio-frequency plasma functionalization of carbon nanotubes surface O_2, NH_3, and CF_4 treatments. J Appl Phys 2005;98:074308.
[29] Ruelle B, Peeterbroeck S, Gouttebaron R, Godfroid T, Monteverde F, Dauchot J-P, et al. Functionalization of carbon nanotubes by atomic nitrogen formed in a microwave plasma Ar + N_2 and subsequent poly([varepsilon]-caprolactone) grafting. J Mater Chem 2007;17:157–9.
[30] Valentini L, Puglia D, Armentano I, Kenny J. Sidewall functionalization of single-walled carbon nanotubes through CF_4 plasma treatment and subsequent reaction with aliphatic amines. Chem Phys Lett 2005;403:385–9.
[31] Williams J, Broughton W, Koukoulas T, Rahatekar S. Plasma treatment as a method for functionalising and improving dispersion of carbon nanotubes in epoxy resins. J Mater Sci 2013;48:1005–13.
[32] Wang S, Liang Z, Liu T, Wang B, Zhang C. Effective amino-functionalization of carbon nanotubes for reinforcing epoxy polymer composites. Nanotechnology 2006;17:1551.
[33] Wicks SS, de Villoria RG, Wardle BL. Interlaminar and intralaminar reinforcement of composite laminates with aligned carbon nanotubes. Compos Sci Technol 2010;70:20–8.
[34] Davis DC, Whelan BD. An experimental study of interlaminar shear fracture toughness of a nanotube reinforced composite. Compos Part B: Eng 2011;42:105–16.
[35] Zhu Y, Bakis CE, Adair JH. Effects of carbon nanofiller functionalization and distribution on interlaminar fracture toughness of multi-scale reinforced polymer composites. Carbon 2012;50:1316–31.
[36] Joshi SC, Dikshit V. Enhancing interlaminar fracture characteristics of woven CFRP prepreg composites through CNT dispersion. J Compos Mater 2012;46:665–75.
[37] Warrier A, Godara A, Rochez O, Mezzo L, Luizi F, Gorbatikh L, et al. The effect of adding carbon nanotubes to glass/epoxy composites in the fibre sizing and/or the matrix. Compos Part A: Appl Sci Manuf 2010;41:532–8.
[38] da Costa EFR, Skordos AA, Partridge IK, Rezai A. Rtm processing and electrical performance of carbon nanotube modified epoxy/fibre composites. Compos Part A: Appl Sci Manuf 2012;43:593–602.
[39] Bayer Materials Science Baytubes C150P Data sheet. <www.bayer.com>; 2012.
[40] Haydale Ltd., Clos Fferws, Parc Hendre, Carmarthenshire, SA18 3BL, UK. www.Haydale.com; 2013.
[41] Walters I. Methods and apparatus for particle processing with plasma. Patent No. EP2440323 (A1). <worldwide.espacenet.com>; 2010.
[42] Walters I, Williams M. Particulate materials, composites comprising them, preparation and uses thereof. Patent No. WO2012076853 (A1). <worldwide.espacenet.com>; 2012.
[43] Hexcel, Hexcel 913 data sheet. <www.hexcel.com>; 2012.
[44] Henry DC. The cataphoresis of suspended particles. Part I. The equation of cataphoresis. Proc Royal Soc Lond Ser A 1931;133:106–29.
[45] Malvern Instruments Ltd., UK, Malvern Zetasizer Nanoseries, Software version 6.20, Manual: MAN0317-5.0 <www.Malvern.com>; 2009.
[46] Sun Z, Nicolosi V, Rickard D, Bergin SD, Aherne D, Coleman JN. Quantitative evaluation of surfactant-stabilized single-walled carbon nanotubes: dispersion quality and its correlation with zeta potential. J Phys Chem C 2008;112:10692–9.
[47] White B, Banerjee S, O'Brien S, Turro NJ, Herman IP. Zeta-potential measurements of surfactant-wrapped individual single-walled carbon nanotubes. J Phys Chem C 2007;111:13684–90.
[48] Haynes WM, editor. CRC handbook of chemistry and physics. group: Taylor & Francis; 2011.
[49] ASTM-D5528-01. Mode I interlaminar fracture toughness of unidirectional fiber-reinforced polymer matrix composites, technical report, American Society for Testing and Materials International; 2007.
[50] Hu H, Yu A, Kim E, Zhao B, Itkis ME, Bekyarova E, et al. Influence of the zeta potential on the dispersability and purification of single-walled carbon nanotubes. J Phys Chem B 2005;109:11520–4.
[51] Zhao L, Gao L. Stability of multi-walled carbon nanotubes dispersion with copolymer in ethanol. Colloids Surf A: Physicochem Eng Aspects 2003;224:127–34.
[52] Kim B, Park H, Sigmund WM. Electrostatic interactions between shortened multiwall carbon nanotubes and polyelectrolytes. Langmuir 2003;19:2525–7.
[53] Yu A, Bekyarova E, Itkis ME, Fakhrutdinov D, Webster R, Haddon RC. Application of centrifugation to the large-scale purification of electric arc-produced single-walled carbon nanotubes. J Am Chem Soc 2006;128:9902–8.
[54] Gojny F, Wichmann M, Koepke U, Fiedler B, Schulte K. Carbon nanotube-reinforced epoxy-composites: enhanced stiffness and fracture toughness at low nanotube content. Compos Sci Technol 2004;64:2363–71.
[55] Bradley WL, Cohen RN. Matrix deformation and fracture in graphite reinforced epoxies. ASTM STP36316S 1985:389–410.
[56] Johnson PMWS. Investigation of fiber bridging in double cantilever beam specimens. J Compos Technol Res 1987;9:10–3.
[57] Agius S, Magniez K, Fox B. Fracture behaviour of a rapidly cured polyethersulfone toughened carbon fibre/epoxy composite. Compos Struct 2010;92:2119–27 [Fifteenth international conference on composite structure].